Strong Intrinsic Longitudinal Coupling in Circuit Quantum Electrodynamics

Potts, C. A.; Dekker, R. C.; Deve, S.; Strijbis, E. W.; Steele, G. A.

DOI
10.1103/PhysRevLett.134.153603

Publication date
2025

Document Version
Final published version

Published in
Physical review letters

Strong Intrinsic Longitudinal Coupling in Circuit Quantum Electrodynamics

C. A. Potts,[1,2,3,*] R. C. Dekker,[1] S. Deve,[1] E. W. Strijbis,[1] and G. A. Steele[1,†]
[1]Kavli Institute of Nanoscience, Delft University of Technology, PO Box 5046, 2600 GA Delft, The Netherlands
[2]Niels Bohr Institute, University of Copenhagen, Blegdamsvej 17, 2100 Copenhagen, Denmark
[3]NNF Quantum Computing Programme, Niels Bohr Institute, University of Copenhagen, Denmark

(Received 16 December 2024; revised 19 February 2025; accepted 24 March 2025; published 18 April 2025)

Radiation-pressure interactions between harmonic oscillators have enabled exquisite measurement precision and control, made possible by using strong sideband drives, enhancing the coupling rate while also linearizing the interaction. In this Letter, we demonstrate a strong intrinsic longitudinal coupling, a circuit quantum electrodynamics analog of the radiation-pressure interaction, between a transmon qubit and a linear microwave resonator. A red-detuned sideband drive results in an on-demand Jaynes-Cummings interaction with a high on-off ratio. We measure a longitudinal coupling rate an order of magnitude larger than all decay rates, placing the device in the strong coupling regime. The intrinsic longitudinal interaction demonstrated here will enable the development of high-connectivity quantum information processing hardware and the exploration of the gravitational decoherence of quantum objects.

DOI: 10.1103/PhysRevLett.134.153603

Introduction—Radiation-pressure interactions arise when the frequency of a system is modulated by the coordinate of a second system. Interactions of this type between harmonic oscillators have provided the foundation for a wide range of groundbreaking experiments in the last several decades. A canonical example is that of cavity optomechanics [1] but includes related fields such as cavity magnomechanics [2–5], photon-pressure coupling [6–10], and the center of mass motion of trapped ions [11,12]. Such interactions have enabled scientific achievements such as ground-state cooling of mechanical objects [13–15], the generation of deterministic mechanical entanglement [16], microwave-to-optical frequency conversion [17,18], and quantum nondemolition measurements [19,20]. These demonstrations have relied on enhancing the typically low coupling rate via strong sideband drive tones, linearizing the intrinsically nonlinear interaction.

In the context of superconducting qubits, the interaction analogous to radiation pressure known as "longitudinal coupling" has recently been proposed as a new paradigm for quantum information processing [21,22], with exciting potential applications for quantum processors [23,24], and has been widely demonstrated in ion-trap hardware [11,12,25]. For example, longitudinal coupling could allow for all-to-all qubit connectivity and pure quantum nondemolition qubit readout [26–28]. The application of coherent drives has enabled an effective longitudinal coupling [29], which has been used to demonstrate efficient qubit readout [30,31]. However, despite this interest, limited experimental progress on pure longitudinal coupling in superconducting circuits has been made, with most experimental realizations suffering from dominant parasitic transverse coupling spoiling the pure longitudinal nature [32].

In this Letter, we demonstrate an entirely hardware-realized *pure longitudinal* interaction between a superconducting qubit and a linear microwave resonator circuit. The device implements longitudinal coupling with negligible transverse coupling encoded directly in the circuit design. The interaction between the qubit and the resonator is engineered by threading the magnetic flux generated by the linear resonator through a superconducting quantum interference device (SQUID) [6,7,22], forming the inductance of the qubit. Using a sideband drive, we induce an effective Jaynes-Cummings interaction in the strong coupling limit that can be dynamically controlled with a high on-off ratio. Furthermore, the ac-Stark shift of the qubit provides an absolute photon number calibration [33], allowing for the extraction of the longitudinal coupling rate. We find a longitudinal coupling rate, $g_0 = 2\pi \times 11.9$ MHz, 2 orders of magnitude larger than the largest dissipation rate of the system, placing our system deep in the single-photon strong coupling regime [1].

The single-photon strong coupling regime has long been sought as it fully utilizes the inherent nonlinearity of the radiation-pressure interaction [34,35]. Since linear interactions can only perform bilinear operations on Gaussian states, single-photon strong coupling would allow the dissipative engineering of states with Wigner negativity, such as described in the protocol for the generation of Schrödinger cat states [36]. Moreover, the longitudinal interaction allows a large number of photons to be driven

*Contact author: clinton.potts@nbi.ku.dk
†Contact author: g.a.steele@tudelft.nl

into the linear resonator, unlike in conventional transverse circuit quantum electrodynamics (cQED) [37]. Therefore, combining longitudinal cQED with conventional optomechanics integrated within the linear resonator will enable the generation of mechanical Schrödinger cat states, via a double state swap procedure, to explore gravity's effect on quantum mechanics [38].

Device design—The device consists of a modified transmon qubit coupled to two superconducting resonators, all with frequencies in the gigahertz range. The device's full circuit schematic can be seen in Fig. 1. All circuits are fabricated from niobium titanium nitride [39]; the fabrication details are outlined in Supplemental Material [40]. A $\lambda/2$ coplanar waveguide resonator (CPW) labeled $\hat{c}$ is capacitively coupled to the qubit and acts as a standard readout resonator for qubit measurements and state preparation [37,47]. It has a frequency $\omega_c = 2\pi \times 7.612$ GHz, a qubit-photon coupling rate $g_{ac} = 2\pi \times 118$ MHz, an internal and external coupling rate of $\kappa_{int,c} = 2\pi \times 72.8$ kHz and $\kappa_{ext,c} = 2\pi \times 673.8$ kHz.

The linear resonator labeled $\hat{b}$ consists of a large interdigitated capacitor shunted with a thin inductor wire. The linear resonator has a resonance frequency $\omega_b = 2\pi \times 4.347$ GHz, an internal and external coupling rate of $\kappa_{int,b} = 2\pi \times 28.0$ kHz and $\kappa_{ext,b} = 2\pi \times 88.6$ kHz, and a residual parasitic dipolar coupling to the qubit $g_{ab} = 2\pi \times 1.4$ MHz. The parasitic capacitive coupling was minimized by careful qubit design and results in a critical photon number at the qubit operational point of $n_{crit} \equiv \Delta^2/4g_{ab}^2 \approx 350\,000$, where Δ is the qubit-linear resonator detuning [37]. The reduced hybridization between the qubit and linear resonator is an essential feature of the qubit design; the low coupling rate g_{ab} allows relatively large coherent drives to be applied to the linear resonator. We observe a bare-to-dressed transition of the linear resonator with a steady state drive $|\langle\hat{b}\rangle|^2 \approx 20\,000$, which is approximately an order of magnitude smaller than the critical photon number. However, we expect the number of drive photons to increase significantly even with moderate reductions of the parasitic dipolar coupling [48]. These large coherent drives will be necessary if the linear resonator is replaced with a cavity optomechanical device since large coherent tones are required for mechanical state manipulation [14].

Finally, the qubit labeled $\hat{a}$ is a modified pocket-style transmon qubit with Manhattan-style aluminum aluminum-oxide junctions [49]. As seen in Fig. 1, one of the capacitor pads of the transmon is split and wrapped around the other, and the SQUID loop is extended away from the capacitor pads. The SQUID loop is placed ~1 μm from the thin inductor wire of the linear circuit. This design was implemented to reduce the electric dipole moment of the qubit, minimizing the parasitic dipole coupling to the linear resonator, as discussed previously. We believe the parasitic coupling likely results from junction asymmetry

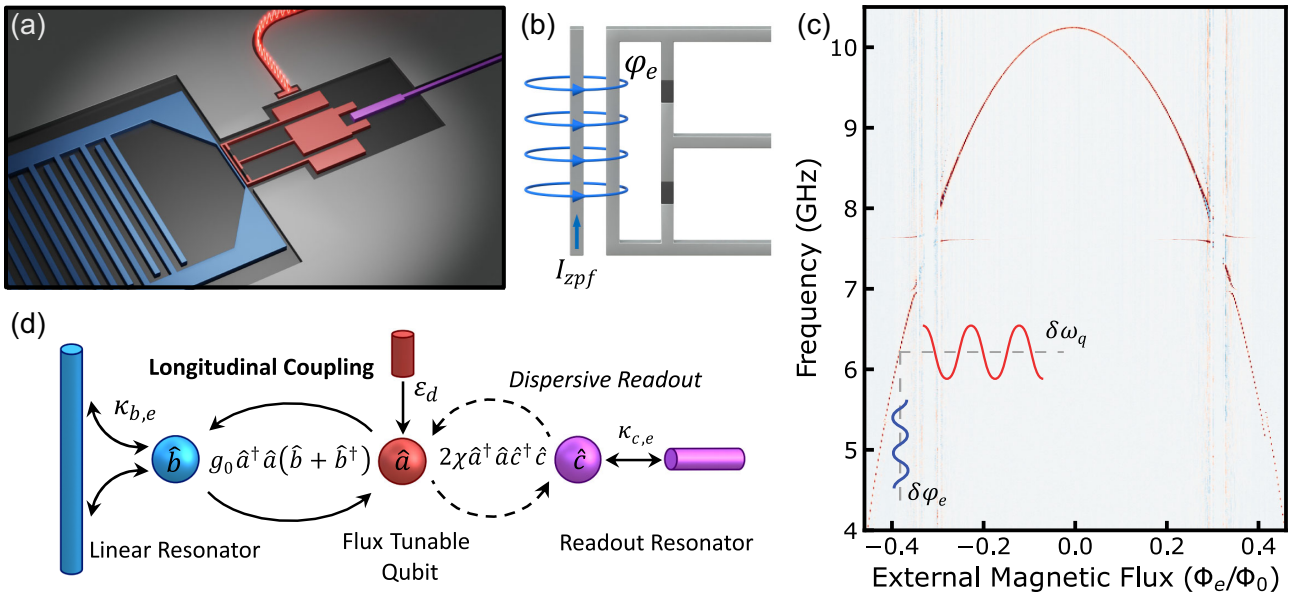

FIG. 1. A superconducting quantum circuit with pure longitudinal coupling. (a) A rendering of the superconducting device. (b) Schematic depiction of the longitudinal coupling mechanism. Zero-point current in the linear resonator generates a magnetic flux that modulates the qubit frequency. (c) Qubit two-tone spectroscopy as a function of the external magnetic flux. The qubit has a sweet spot frequency of 10.2 GHz. The magnetic flux generated by currents in the linear resonator modulates the qubit frequency, resulting in longitudinal coupling. Data near the readout resonator frequency of 7.6 GHz is excluded due to the qubit resonator hybridization. (d) Schematic diagram of the device. The qubit $\hat{a}$ is coupled via a longitudinal interaction to the linear resonator $\hat{b}$ and coupled capacitively to a CPW resonator $\hat{c}$.

resulting in finite current through the linear inductor of the SQUID and charging of the surrounding ground plane.

A coil mounted below the sample provides an external magnetic field that can tune the frequency of the qubit; see Fig. 1(c). During this work, the qubit was operated at a frequency $\omega_q(\Phi_e) \sim 2\pi \times 6.10$ GHz, where Φ_e is the static external magnetic flux thread through the SQUID. The qubit can be driven via a direct XY-drive line, which was designed to be weakly coupled such that the Purcell limited linewidth κ_{pur} is much less than the qubit linewidth γ_q. Finally, we measured a T_2^* limited linewidth $\gamma_q = 2\pi \times 677$ kHz; qubit characterization is described within Supplemental Material. The chip is mounted on the baseplate of a commercial dilution refrigerator operating with a base temperature of $T \sim 15$ mK. For details about the measurement and setup, see Supplemental Material [40].

Operational principle—We model the qubit as a Kerr oscillator with a large anharmonicity [37], the bare Hamiltonian of the system can be written in the form

$$\hat{\mathcal{H}}_0/\hbar = \omega_q(\Phi_e)\hat{a}^\dagger\hat{a} + \frac{\alpha}{2}\hat{a}^\dagger\hat{a}^\dagger\hat{a}\,\hat{a} + \omega_b\hat{b}^\dagger\hat{b}. \tag{1}$$

Here, $\alpha = -388$ MHz is the qubit anharmonicity at the operation point, $\hat{a}^{(\dagger)}$ and $\hat{b}^{(\dagger)}$ are the qubit and linear resonator annihilation (creation) operators, respectively.

Current flowing through the inductor wire of the linear resonator generates an oscillating magnetic flux through the SQUID loop, modulating the qubit's frequency and inducing the coupling between the qubit and linear resonator; see Figs. 1(b), (c). It can be shown, after some algebraic manipulation and keeping only first-order terms (see Supplemental Material) that the interaction can be written in the simple form [40]

$$\hat{\mathcal{H}}_{int}/\hbar = g_0\hat{a}^\dagger\hat{a}(\hat{b} + \hat{b}^\dagger). \tag{2}$$

Here, g_0 is the longitudinal coupling rate and is given by

$$g_0 = \frac{\partial\omega_q}{\partial\Phi}\Phi_{zpf}, \tag{3}$$

where $\partial\omega_q/\partial\Phi$ is the qubit's flux sensitivity at the operational point, and Φ_{zpf} is the magnetic flux thread through the SQUID loop generated by the zero-point current fluctuations of the linear resonator. The zero-point flux can be estimated from the mutual inductance and the zero-point fluctuations in the current given by $I_{zpf} = \sqrt{\hbar\omega_b/2L_b} \approx 36.8$ nA; with $\Phi_{zpf} = MI_{zpf}$. The mutual inductance can be estimated via the Biot-Savart law and gives $M \approx 25.9$ pH; therefore, we estimate the zero-point magnetic flux to have a value $\Phi_{zpf} \approx 461\mu\Phi_0$. We have normalized the magnetic flux in units of $\Phi_0 = h/(2e)$. At the qubit operational point, the flux sensitivity $\partial\omega_q/\partial\Phi = 2\pi \times 26.0$ GHz$/\Phi_0$, thus we can estimate the longitudinal coupling rate to have a value $g_0 \approx 2\pi \times 12.0$ MHz.

On-demand Jaynes-Cummings—The on-demand drive-induced Jaynes-Cummings interaction was implemented using a sideband drive tone tuned to the difference frequency between the two coupled oscillators; see Fig. 2(a). In cavity optomechanics, the sideband drive is typically nearly resonant with the optical cavity, as mechanical frequencies are 1–10 MHz for most electromechanical systems [13,15]. However, this device operates in a vastly different parameter regime. The sideband drive frequency is below both the qubit and linear resonator frequencies. We should emphasize that we are driving single-photon sideband transitions and *not* the two-photon sideband transitions used in conventional cQED [50].

We can linearize the Hamiltonian about the sideband drive tone with frequency $\omega_d \approx \omega_q - \omega_b$ tuned near the red

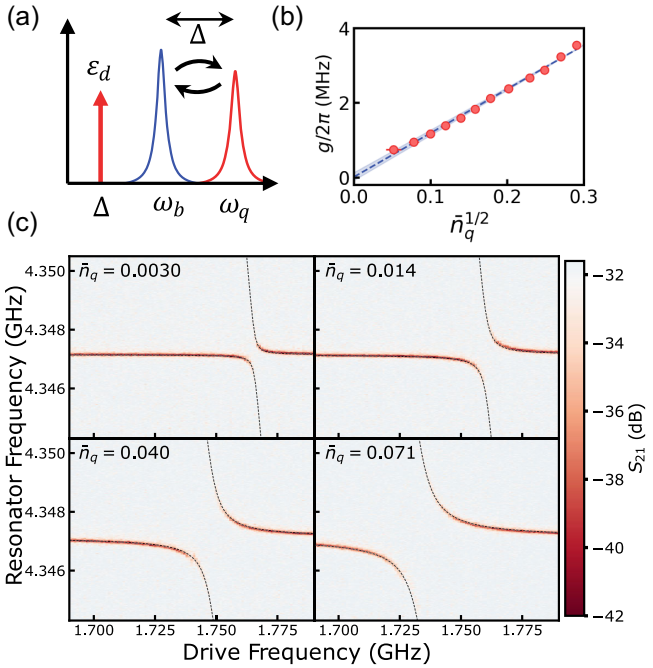

FIG. 2. On-demand strong coupling by driving the longitudinal interaction. (a) Schematic diagram of the relative frequencies of the qubit (red), the linear resonator (blue), and the sideband drive (red). (b) Cavity-enhanced coupling rates extracted from the normal mode spectra at different sideband drive powers. The coupling rates are plotted as a function of the square root sideband photon number. The red points are data, and the blue dashed line is a linear fit to the data. The blue shaded area accounts for uncertainty in the bare qubit frequency. The photon number was calibrated using the ac-Stark shift. (c) The measured avoided level crossings of the linear resonator as a function of the sideband drive frequency. Starting from the top left, the drive powers considered here were $P_{sb} = 3.3$, 8.3, 12.3, 14.4 dBm, set at the source. The calibrated average number of sideband photons is printed in the top left of each panel. The dashed line is a fit; see Supplemental Material for details.

sideband applied via the XY-drive line to the qubit. In a displaced frame corotating with the drive, we can linearize by defining $\hat{a} = \langle \hat{a} \rangle + \delta\hat{a}$; doing so, we can define the enhanced coupling rate as $g = g_0|\langle \hat{a} \rangle|$, and $\bar{n}_q = |\langle \hat{a} \rangle|^2$ is the average sideband steady-state population of the qubit. The interaction Hamiltonian given in Eq. (2) can be written, taking the two-level approximation of the transmon and applying the rotating wave approximation, as

$$\hat{\mathcal{H}}_{\text{int}}/\hbar = g(\hat{\sigma}_- \hat{b}^\dagger + \hat{\sigma}_+ \hat{b}), \tag{4}$$

where $\hat{\sigma}_\pm$ are the qubit raising and lowering operators. The linearization process results in an on-demand drive-induced Jaynes-Cummings interaction created by the sideband drive; see Supplemental Material for a full derivation [40].

The interaction is experimentally investigated by sweeping a sideband drive near the red sideband and probing the linear resonator with less than a single photon on average to remain in the single-excitation manifold of the Jaynes-Cummings ladder [51]. We observe a series of avoided level crossings with a correspondingly increasing coupling rate as a function of increasing sideband power and a shift to lower frequencies, as shown in Fig. 2(c). We can extract the cavity-enhanced coupling rate g from the avoided level crossings. However, we require an absolute calibration of the photon number to determine the longitudinal coupling rate. Conventionally, this is achieved by varying the temperature of the dilution refrigerator and performing thermal calibration [13], or applying a known modulation and carefully measuring all loss and gain within the system [52,53].

Instead, we can use the ac-Stark shift of the qubit for direct photon number calibration. As we increase the sideband drive power, the qubit experiences an increasing ac-Stark shift. The magnitude of the Stark shift is directly related to the average number of sideband photons in the qubit. One must take care when interpreting the Stark shift, which is why we initially modeled the qubit as a Kerr oscillator. Since the sideband drive is far detuned, the counter-rotating terms, known as the Bloch-Siegert shift [33], and the qubit anharmonicity contribute significantly. Considering the steady state of the Kerr oscillator and the ac-Stark shift, the steady-state qubit population for each sideband power can be directly calculated.

The value of the longitudinal coupling rate can be determined by considering the cavity-enhanced coupling rate as a function of the square root of the number of steady-state sideband photons, as seen in Fig. 2(b). Importantly, the relationship is linear, suggesting our approximations are valid and hold even for steady-state populations below the single-photon level, and the data has a y intercept of zero, which is expected since the cavity-enhanced coupling should vanish for no sideband drive. The value of the longitudinal coupling rate can be determined from the slope, giving a value of $g_0 = 2\pi \times 11.9 \pm 0.3$ MHz, which is in excellent agreement with our theoretical prediction and well within the single-photon strong coupling regime.

Rabi oscillations—Finally, to demonstrate the coherent nature of the interaction, we measure vacuum Rabi oscillations between the qubit and the linear resonator. The qubit is first prepared into its excited state $|e\rangle$ using a 24 ns resonant π pulse. A square wave sideband pulse is applied near the red sideband frequency for a variable time τ. Following the sideband pulse, the qubit state is measured using the capacitively coupled CPW resonator. This protocol is repeated for various sideband drive frequencies and pulse durations, resulting in the vacuum Rabi oscillations shown in Fig. 3. We observe a typical Rabi "chevron" pattern with coherent exchanges between the qubit and the linear resonator. A line cut is fit using a numerical simulation of the Rabi oscillations to confirm our linear model; see Supplemental Material [40]. From the numerical simulation, we can extract the coupling rate $g/2\pi = 2.76 \pm 0.03$ MHz, [54] resulting in a sideband π-pulse duration of $\sim$91 ns; see Fig. 3(b). This is in excellent agreement with the measured normal mode splitting at nominally the same sideband power, $g/2\pi = 2.81 \pm 0.08$ MHz. Finally, we observe transitions to higher excited manifolds of the Jaynes-Cummings ladder by preparing the linear oscillator in the Fock state $|1\rangle$ using a sideband π pulse and measuring the Rabi oscillations. We observe a Rabi frequency with a value $g_2 \approx \sqrt{2}g$, as predicted by the Jaynes-Cummings model [54]; see Fig. 3(c).

Outlook—This Letter presents a unique interface between a superconducting qubit and a linear microwave resonator. The interaction was confirmed by performing normal-mode spectroscopy of the hybrid modes induced via a red sideband drive and observing coherent Rabi oscillations. The value of the longitudinal coupling rate was determined by calibrating the sideband drive using the ac-Stark shift. Our device is well within the single-photon strong coupling limit.

The innovative qubit design provides a new platform for testing theories demanding single-photon strong coupling, such as dissipative Schrödinger cat state generation within the microwave resonator [36]. Moreover, the large critical photon number, $n_{\text{crit}} \approx 350\,000$, and the ability to dynamically modulate the coupling should allow for future integration with optomechanics experiments. In such an experiment, the cat state generated within the linear resonator can be swapped into a mechanical oscillator using a strong optomechanical sideband pulse, generating a macroscopic superposition allowing for exotic tests of gravitational decoherence [38]. Such a swap to the mechanical resonator would *not* be possible using conventional Jaynes-Cummings coupling due to the large driving requirements on the linear microwave cavity.

Moreover, this platform may also be used for interesting on-chip quantum optics experiments; for example, at the

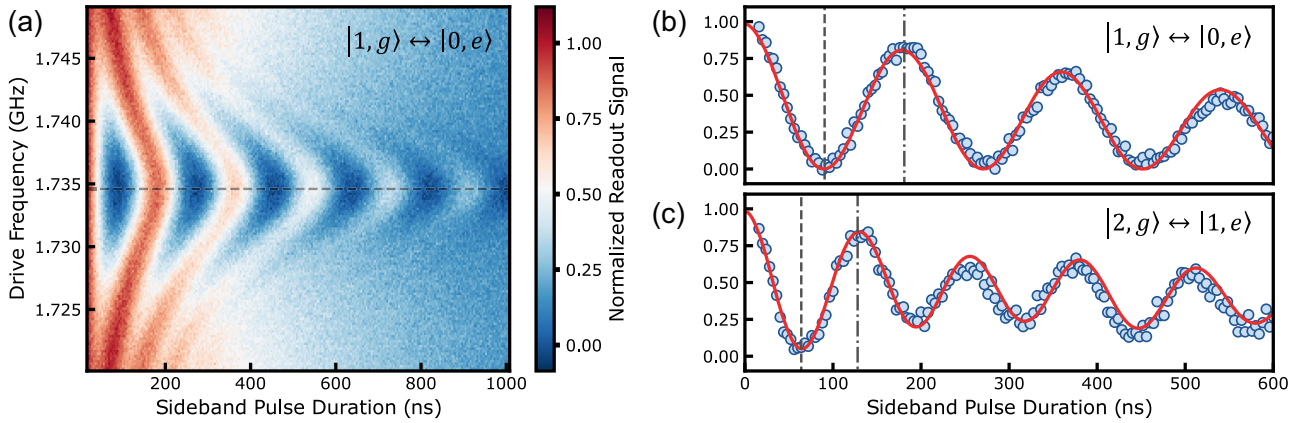

FIG. 3. Observation of coherent swaps of photons up the on-demand Jaynes-Cummings ladder. (a) Rabi chevrons with a single excitation in the system. The normalized output signal is proportional to the excited state probability of the qubit $P_{|e\rangle}$. (b) Line cut of resonant Rabi oscillations for the $|1,g\rangle \leftrightarrow |0,e\rangle$ transition. A Rabi frequency $g = 2\pi \times 2.76$ MHz was used in the numerical simulation. The dashed lines indicate the longitudinal π-pulse duration $t_\pi = 90.5$ ns. The dotted dashed lines indicate the Rabi oscillation period, and the solid red line is a numerical simulation of the Rabi oscillations. (c) Line cut of resonant Rabi oscillations for the $|2,g\rangle \leftrightarrow |1,e\rangle$ transition. An increased Rabi frequency $g_2 \approx \sqrt{2}g$ is observed. The dashed lines indicate the predicted second manifold longitudinal π-pulse duration $t_{\pi,2} = 90.5/\sqrt{2}$ ns. The dotted dashed lines indicate the Rabi oscillation period, and the solid red line is a numerical simulation of the Rabi oscillations.

top sweet spot to first order, the linear coupling should be suppressed, i.e., $g_0 \approx 0$; however, there will remain quadratic coupling of the form $\hat{\mathcal{H}}_q/\hbar = g_q \hat{a}^\dagger \hat{a}(\hat{b} + \hat{b}^\dagger)^2$. Quadratic coupling has been long sought and was an initial driving force for the membrane in the middle experiments [55]. By eliminating linear coupling, the quadratic coupling may allow quantum nondemolition measurement of the photon number within the linear resonator. This enables an on-chip cQED measurement of stochastic photon jumps as they decay from the linear resonator [56,57].

Finally, the longitudinal coupling can be explored as a unique architecture for quantum information systems [21,23,24,26]. Multiple qubits could be coupled to a single bus resonator, and by applying appropriate sideband pulses, sideband drive-mediated qubit-qubit gates may be possible. All qubits connected via the longitudinal interaction to a single bus resonator would allow a fully superconducting implementation of efficient quantum computation architectures currently studied using ion traps [58].

Acknowledgments—The authors thank V. A. S. V Bittencourt and M. Kjaergaard for helpful discussions and Enrique Sahagun for the device rendering [59]. C. A. P. acknowledges the support of the Natural Sciences and Engineering Research Council of Canada (NSERC) (PDF-567689-2022) and the Novo Nordisk Foundation, NNF Quantum Computing Programme. R. C. D. acknowledges support from the Netherlands Organisation for Scientific Research (NWO/OCW) as part of the Frontiers of Nanoscience program. This publication is part of the project "Superconducting Electromechanics: Massive superpositions for exploring quantum mechanics and general relativity." Project No. VI.C.212.087 of the research programme VICI round 2021, financed by the Dutch Research Council (NWO).

C. A. P. performed theoretical modeling, performed data analysis, designed the qubit, performed daily supervision of measurements and coordination of the team, wrote the first draft of the manuscript with input from all authors, and incorporated feedback from authors into the final manuscript. R. C. D. designed and simulated the full device layout, developed the fabrication recipe and fabricated the device, performed spectroscopic measurements, contributed to data analysis, and contributed to figure design. S. D. contributed to the verification of theoretical models. S. D. and E. S. performed time-domain qubit measurements and analysis of those measurements. G. A. S. was responsible for conceiving the experiment, overall supervision of the project, and the acquisition of funding for the project. All authors contributed to the formulation of the manuscript storyline and the composition of the figures.

The authors declare no competing interests.

Data availability—The data that support the findings of this article are openly available [60].

[1] M. Aspelmeyer, T. J. Kippenberg, and F. Marquardt, Cavity optomechanics, Rev. Mod. Phys. **86**, 1391 (2014).
[2] X. Zhang, C.-L. Zou, L. Jiang, and H. X. Tang, Cavity magnomechanics, Sci. Adv. **2**, e1501286 (2016).

[3] C. A. Potts, E. Varga, V. A. S. V. Bittencourt, S. Viola-Kusminskiy, and J. P. Davis, Dynamical backaction magnomechanics, Phys. Rev. X **11**, 031053 (2021).
[4] R.-C. Shen, J. Li, Z.-Y. Fan, Y.-P. Wang, and J. Q. You, Mechanical bistability in Kerr-modified cavity magnomechanics, Phys. Rev. Lett. **129**, 123601 (2022).
[5] C. A. Potts, Y. Huang, V. A. S. V. Bittencourt, S. Viola-Kusminskiy, and J. P. Davis, Dynamical backaction evading magnomechanics, Phys. Rev. B **107**, L140405 (2023).
[6] C. Eichler and J. R. Petta, Realizing a circuit analog of an optomechanical system with longitudinally coupled superconducting resonators, Phys. Rev. Lett. **120**, 227702 (2018).
[7] D. Bothner, I. C. Rodrigues, and G. A. Steele, Photon-pressure strong coupling between two superconducting circuits, Nat. Phys. **17**, 85 (2021).
[8] I. C. Rodrigues, D. Bothner, and G. A. Steele, Cooling photon-pressure circuits into the quantum regime, Sci. Adv. **7**, eabg6653 (2021).
[9] I. C. Rodrigues, G. A. Steele, and D. Bothner, Parametrically enhanced interactions and nonreciprocal bath dynamics in a photon-pressure Kerr amplifier, Sci. Adv. **8**, eabq1690 (2022).
[10] I. C. Rodrigues, G. A. Steele, and D. Bothner, Photon pressure with an effective negative mass microwave mode, Phys. Rev. Lett. **132**, 203603 (2024).
[11] D. Leibfried, B. DeMarco, V. Meyer, D. Lucas, M. Barrett, J. Britton, W. M. Itano, B. Jelenković, C. Langer, T. Rosenband *et al.*, Experimental demonstration of a robust, high-fidelity geometric two ion-qubit phase gate, Nature (London) **422**, 412 (2003).
[12] P. C. Haljan, K.-A. Brickman, L. Deslauriers, P. J. Lee, and C. Monroe, Spin-dependent forces on trapped ions for phase-stable quantum gates and entangled states of spin and motion, Phys. Rev. Lett. **94**, 153602 (2005).
[13] Y. Seis, T. Capelle, E. Langman, S. Saarinen, E. Planz, and A. Schliesser, Ground state cooling of an ultracoherent electromechanical system, Nat. Commun. **13**, 1507 (2022).
[14] J. D. Teufel, T. Donner, D. Li, J. W. Harlow, M. Allman, K. Cicak, A. J. Sirois, J. D. Whittaker, K. W. Lehnert, and R. W. Simmonds, Sideband cooling of micromechanical motion to the quantum ground state, Nature (London) **475**, 359 (2011).
[15] A. Noguchi, R. Yamazaki, M. Ataka, H. Fujita, Y. Tabuchi, T. Ishikawa, K. Usami, and Y. Nakamura, Ground state cooling of a quantum electromechanical system with a silicon nitride membrane in a 3D loop-gap cavity, New J. Phys. **18**, 103036 (2016).
[16] S. Kotler, G. A. Peterson, E. Shojaee, F. Lecocq, K. Cicak, A. Kwiatkowski, S. Geller, S. Glancy, E. Knill, R. W. Simmonds *et al.*, Direct observation of deterministic macroscopic entanglement, Science **372**, 622 (2021).
[17] R. W. Andrews, R. W. Peterson, T. P. Purdy, K. Cicak, R. W. Simmonds, C. A. Regal, and K. W. Lehnert, Bidirectional and efficient conversion between microwave and optical light, Nat. Phys. **10**, 321 (2014).
[18] W. Jiang, C. J. Sarabalis, Y. D. Dahmani, R. N. Patel, F. M. Mayor, T. P. McKenna, R. Van Laer, and A. H. Safavi-Naeini, Efficient bidirectional piezo-optomechanical transduction between microwave and optical frequency, Nat. Commun. **11**, 1166 (2020).
[19] J. B. Hertzberg, T. Rocheleau, T. Ndukum, M. Savva, A. A. Clerk, and K. C. Schwab, Back-action-evading measurements of nanomechanical motion, Nat. Phys. **6**, 213 (2010).
[20] F. Lecocq, J. B. Clark, R. W. Simmonds, J. Aumentado, and J. D. Teufel, Quantum nondemolition measurement of a nonclassical state of a massive object, Phys. Rev. X **5**, 041037 (2015).
[21] P.-M. Billangeon, J. S. Tsai, and Y. Nakamura, Circuit-QED-based scalable architectures for quantum information processing with superconducting qubits, Phys. Rev. B **91**, 094517 (2015).
[22] J. R. Johansson, G. Johansson, and F. Nori, Optomechanical-like coupling between superconducting resonators, Phys. Rev. A **90**, 053833 (2014).
[23] S. Richer and D. DiVincenzo, Circuit design implementing longitudinal coupling: A scalable scheme for superconducting qubits, Phys. Rev. B **93**, 134501 (2016).
[24] X. Wang, A. Miranowicz, and F. Nori, Ideal quantum nondemolition readout of a flux qubit without purcell limitations, Phys. Rev. Appl. **12**, 064037 (2019).
[25] A. Sørensen and K. Mølmer, Entanglement and quantum computation with ions in thermal motion, Phys. Rev. A **62**, 022311 (2000).
[26] N. Didier, J. Bourassa, and A. Blais, Fast quantum nondemolition readout by parametric modulation of longitudinal qubit-oscillator interaction, Phys. Rev. Lett. **115**, 203601 (2015).
[27] A. A. Chapple, A. McDonald, M. H. Munoz-Arias, and A. Blais, Robustness of longitudinal transmon readout to ionization, arXiv:2412.07734.
[28] A. Chessari, E. A. Rodríguez-Mena, J. C. Abadillo-Uriel, V. Champain, S. Zihlmann, R. Maurand, Y.-M. Niquet, and M. Filippone, Unifying Floquet theory of longitudinal and dispersive readout, Phys. Rev. Lett. **134**, 037003 (2025).
[29] A. Eickbusch, V. Sivak, A. Z. Ding, S. S. Elder, S. R. Jha, J. Venkatraman, B. Royer, S. M. Girvin, R. J. Schoelkopf, and M. H. Devoret, Fast universal control of an oscillator with weak dispersive coupling to a qubit, Nat. Phys. **18**, 1464 (2022).
[30] J. Ikonen, J. Goetz, J. Ilves, A. Keränen, A. M. Gunyho, M. Partanen, K. Y. Tan, D. Hazra, L. Grönberg, V. Vesterinen *et al.*, Qubit measurement by multichannel driving, Phys. Rev. Lett. **122**, 080503 (2019).
[31] S. Touzard, A. Kou, N. Frattini, V. Sivak, S. Puri, A. Grimm, L. Frunzio, S. Shankar, and M. Devoret, Gated conditional displacement readout of superconducting qubits, Phys. Rev. Lett. **122**, 080502 (2019).
[32] I. Chiorescu, P. Bertet, K. Semba, Y. Nakamura, C. Harmans, and J. Mooij, Coherent dynamics of a flux qubit coupled to a harmonic oscillator, Nature (London) **431**, 159 (2004).
[33] B.-m. Ann, W. Kessels, and G. A. Steele, Sideband transitions in a two-mode Josephson circuit driven beyond the rotating-wave approximation, Phys. Rev. Res. **3**, 033004 (2021).
[34] A. Nunnenkamp, K. Børkje, and S. M. Girvin, Single-photon optomechanics, Phys. Rev. Lett. **107**, 063602 (2011).
[35] A. Nunnenkamp, K. Børkje, and S. M. Girvin, Cooling in the single-photon strong-coupling regime of cavity optomechanics, Phys. Rev. A **85**, 051803(R) (2012).

[36] B. D. Hauer, J. Combes, and J. D. Teufel, Nonlinear sideband cooling to a cat state of motion, Phys. Rev. Lett. **130**, 213604 (2023).
[37] P. Krantz, M. Kjaergaard, F. Yan, T. P. Orlando, S. Gustavsson, and W. D. Oliver, A quantum engineer's guide to superconducting qubits, Appl. Phys. Rev. **6**, 021318 (2019).
[38] M. F. Gely and G. A. Steele, Superconducting electromechanics to test Diosi-Penrose effects of general relativity in massive superpositions, AVS Quantum Sci. **3**, 035601 (2021).
[39] D. J. Thoen, B. G. C. Bos, E. Haalebos, T. Klapwijk, J. Baselmans, and A. Endo, Superconducting NbTiN thin films with highly uniform properties over a 100 mm wafer, IEEE Trans. Appl. Supercond. **27**, 1 (2016).
[40] See Supplemental Material at http://link.aps.org/supplemental/10.1103/PhysRevLett.134.153603 for information on fabrication, simulations, and theoretical modeling, which includes Refs. [41–46].
[41] R. Igreja and C. J. Dias, Analytical evaluation of the interdigital electrodes capacitance for a multi-layered structure, Sens. Actuators A **112**, 291 (2004).
[42] J. R. Johansson, P. D. Nation, and F. Nori, Qutip: An open-source Python framework for the dynamics of open quantum systems, Comput. Phys. Commun. **183**, 1760 (2012).
[43] T. Abad, J. Fernández-Pendás, A. Frisk Kockum, and G. Johansson, Universal fidelity reduction of quantum operations from weak dissipation, Phys. Rev. Lett. **129**, 150504 (2022).
[44] D. Zoepfl, M. L. Juan, N. Diaz-Naufal, C. M. F. Schneider, L. F. Deeg, A. Sharafiev, A. Metelmann, and G. Kirchmair, Kerr enhanced backaction cooling in magnetomechanics, Phys. Rev. Lett. **130**, 033601 (2023).
[45] A. Reiserer and G. Rempe, Cavity-based quantum networks with single atoms and optical photons, Rev. Mod. Phys. **87**, 1379 (2015).
[46] C. Gardiner and P. Zoller, *Quantum Noise: A Handbook of Markovian and non-Markovian Quantum Stochastic Methods with Applications to Quantum Optics* (Springer Science & Business Media, Berlin, Heidelberg, 2004).
[47] A. Blais, A. L. Grimsmo, S. M. Girvin, and A. Wallraff, Circuit quantum electrodynamics, Rev. Mod. Phys. **93**, 025005 (2021).
[48] M. Boissonneault, J. M. Gambetta, and A. Blais, Dispersive regime of circuit QED: Photon-dependent qubit dephasing and relaxation rates, Phys. Rev. A **79**, 013819 (2009).
[49] Qiskit contributors, Qiskit: An Open-source Framework for Quantum Computing, 10.5281/zenodo.2573505 (2023).
[50] A. Wallraff, D. I. Schuster, A. Blais, J. M. Gambetta, J. Schreier, L. Frunzio, M. H. Devoret, S. M. Girvin, and R. J. Schoelkopf, Sideband transitions and two-tone spectroscopy of a superconducting qubit strongly coupled to an on-chip cavity, Phys. Rev. Lett. **99**, 050501 (2007).
[51] J. M. Fink, M. Göppl, M. Baur, R. Bianchetti, P. J. Leek, A. Blais, and A. Wallraff, Climbing the Jaynes–Cummings ladder and observing its nonlinearity in a cavity QED system, Nature (London) **454**, 315 (2008).
[52] M. L. Gorodetksy, A. Schliesser, G. Anetsberger, S. Deleglise, and T. J. Kippenberg, Determination of the vacuum optomechanical coupling rate using frequency noise calibration, Opt. Express **18**, 23236 (2010).
[53] A. J. R. MacDonald, B. D. Hauer, X. Rojas, P. H. Kim, G. G. Popowich, and J. P. Davis, Optomechanics and thermometry of cryogenic silica microresonators, Phys. Rev. A **93**, 013836 (2016).
[54] M. Hofheinz, E. M. Weig, M. Ansmann, R. C. Bialczak, E. Lucero, M. Neeley, A. O'connell, H. Wang, J. M. Martinis, and A. N. Cleland, Generation of Fock states in a superconducting quantum circuit, Nature (London) **454**, 310 (2008).
[55] A. Nunnenkamp, K. Børkje, J. G. E. Harris, and S. M. Girvin, Cooling and squeezing via quadratic optomechanical coupling, Phys. Rev. A **82**, 021806(R) (2010).
[56] C. Guerlin, J. Bernu, S. Deleglise, C. Sayrin, S. Gleyzes, S. Kuhr, M. Brune, J.-M. Raimond, and S. Haroche, Progressive field-state collapse and quantum non-demolition photon counting, Nature (London) **448**, 889 (2007).
[57] S. Gleyzes, S. Kuhr, C. Guerlin, J. Bernu, S. Deleglise, U. Busk Hoff, M. Brune, J.-M. Raimond, and S. Haroche, Quantum jumps of light recording the birth and death of a photon in a cavity, Nature (London) **446**, 297 (2007).
[58] K. Wright, K. M. Beck, S. Debnath, J. M. Amini, Y. Nam, N. Grzesiak, J.-S. Chen, N. C. Pisenti, M. Chmielewski, C. Collins *et al.*, Benchmarking an 11-qubit quantum computer, Nat. Commun. **10**, 5464 (2019).
[59] Scixel, https://scixel.es/, accessed: 2023-09-28.
[60] Data available at Zenodo 10.5281/zenodo.14501323.